

Spectral affinities in the icy satellites of Saturn

F. Tosi¹, A. Coradini^{1,2}, D. Turrini³, F. Capaccioni², P. Cerroni²,
and G. Filacchione²

¹ INAF-IFSI, Istituto di Fisica dello Spazio Interplanetario,
Via del Fosso del Cavaliere, 100 I-00133 Roma, Italy,
e-mail: federico.tosi@iasf-roma.inaf.it

² INAF-IASF, Istituto di Astrofisica Spaziale e Fisica Cosmica,
Via del Fosso del Cavaliere, 100 I-00133 Roma, Italy

³ CISAS - Centro Interdipartimentale Studi ed Attività Spaziali "G. Colombo",
Via Venezia, 15 I-35131 Padova, Italy

Abstract. Among the icy satellites of Saturn, Iapetus shows one of the most striking dichotomies in the Solar System, its leading hemisphere being significantly darker than the trailing hemisphere.

Thanks to the Cassini/VIMS imaging spectrometer, it is now possible to investigate the spectrum of the Saturn system bodies in a more accurate way and in a wider spectral range than in the past. In this case, the use of statistical techniques such as clustering methods, can help in the automatic classification of the explored surfaces, with the double aim of identifying spectral units on the satellites, to correlate with the surface geology, and emphasizing correlations among spectra from different bodies, like in the case here expounded.

In this work, we present an application of the *G-mode* method to the VIMS visible and infrared spectra of Phoebe, Iapetus and Hyperion. To enforce the result of this spectroscopic classification, a dynamic study has been carried out as well.

Key words. VIMS – G-mode – satellites – Iapetus – Phoebe – Hyperion

1. Introduction

Saturn's satellite Iapetus shows one of the most striking dichotomies in the Solar System, since its leading hemisphere is mantled by a low-albedo (both optical and radar), carbon-like veneer, whereas its trailing hemisphere is much brighter and consistent with exposed water ice. If the exogenous nature of this dark material is accepted, then we need to find the source. In past times, for different reasons, a number of possible sources have been proposed: Phoebe (Soter 1974), Hyperion (Matthews

1992), or even other small dark irregular satellites (Buratti et al. 2002, 2004).

Should the particles be raised from Phoebe, then the Poynting-Robertson drag can be invoked to migrate them towards the inner region of the Saturn system, where they would collide with Iapetus' leading hemisphere because of their retrograde orbits. The major problem of this early model is that the spectrum of Iapetus' leading side is similar to D-type asteroids, a primitive, very low albedo group of bodies exhibiting a typically "reddish" spectrum in the visual region, that is, increasing in reflectance

with increasing wavelength; whereas Phoebe’s spectrum is essentially flat and grey in the visual region, thus similar to C-type bodies (Tholen and Zellner 1983; Buratti et al. 2002). Moreover, its albedo is higher than carbon, particularly in the brighter areas detected by Voyager 2.

In this work, we explored the data acquired in recent times by the Cassini/VIMS instrument with the G-mode classification method, in order to automatically find similarities and/or differences among the visual and infrared spectra of Iapetus, Phoebe and Hyperion.

2. The G-mode method

The *G-mode*, originally conceived in the mid-70s (Coradini et al. 1977), is a multivariate classification method which has been successfully used in the past to classify such different data sets as lunar rock samples, asteroids and planetary surfaces. This method can be used without any *a priori* knowledge of the taxonomic structure of the observations (samples); moreover, independence of variables and samples is not required, although the relationship between variables and samples needs to be known; the instrumental errors can be taken into account; and different levels of classification can be performed.

Because the G-mode is based on a statistical test, the critical value is expressed in terms of the confidence level of the test: the larger the confidence level, the more general is the classification for the errors of the variables. By changing this value it is therefore possible to get different levels of classification and correspondingly different degrees of class homogeneity. Vice versa, for a given confidence level, the classification becomes more general by increasing the errors on the variables.

3. The VIMS instrument

The *Visual and Infrared Mapping Spectrometer* (VIMS) is an imaging spectrometer onboard the Cassini Orbiter spacecraft. VIMS is actually made up of two spectrometers, VIMS-V and VIMS-IR, devoted to the visible and infrared spectral range respectively

(see Brown et al. (2004a) for details). The VIMS data have two spatial dimensions and one spectral dimension: the field of view is scanned line by line, each line is made up by a number of pixels and every pixel has in turn a spectrum sampled in 352 wavelengths ranging from $0.35 \mu\text{m}$ to $5.1 \mu\text{m}$ (96 wavelengths by VIMS-V and 256 by VIMS-IR). The result of the acquisition is a so-called “image cube” (or simply “cube”) (see Fig. 1). In this work, we separately explored both the visible and infrared portions of the selected cubes.

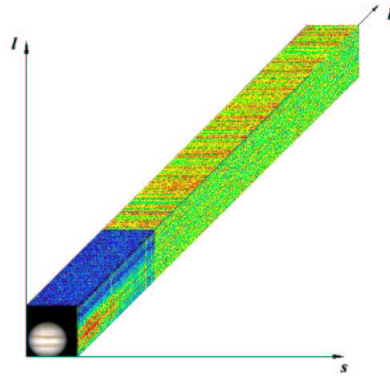


Fig. 1. Structure of the VIMS data. The l and s axes are the spatial dimensions, whereas b is the spectral dimension.

4. The dataset

Multivariate classification methods can be applied to any statistical universe described by N samples, each depending on M variables. In this case, the samples are the VIMS spectra, whereas the variables can be either the spectral channels of the spectrometer, or other parameters such as the band strengths. When using spectral channels as variables, the errors on the variables are assumed to be the instrumental noise, which, for every spectral channel, is given by the inverse of its SNR.

Among the VIMS acquisitions, we selected 3 cubes from the best to-date Cassini flybys with Phoebe (11 June 2004, close flyby), Iapetus (31

December 2004, distant flyby), and Hyperion (26 September 2005, close flyby), respectively. Details about these 3 cubes are shown in Table 1.

Summing the samples from Phoebe, Iapetus and Hyperion, our dataset is made up by 960 spectra. All of the raw spectra have been previously calibrated into Reflectance (Vis) or I/F (IR) spectra by means of the latest instrument transfer function (ITF). Instrumental and random artifacts were taken into account and removed, for both the Vis and IR data, through special destriping and despiking procedures. Whenever possible, the spectra were corrected also for the illumination effects (incidence and emission angles).

5. Results in the Visible range

In the range measured by VIMS-V ($0.35 - 1.05 \mu\text{m}$), no absorption feature can be identified in the spectra of the three satellites; therefore, it is reasonable to expect that any classification is ruled by the continuum trend.

The reflectance spectra of Iapetus, Phoebe and Hyperion were normalized to 1.0 at the wavelength of 549.54 nm (VIMS channel #28), then the G-mode was applied with high confidence level (3.0σ). The classification returns 7 homogeneous types; however, only the first two types are characterized by a large number of samples/spectra (587 and 347 samples respectively), whereas the other clusters are made up by just a few samples.

By plotting the result in a 3D space with axes corresponding to the VIMS spectral channels nearest to the standard R (702.88 nm), G (549.54 nm) and B (439.19 nm) bands, these two big types can be easily recognized (see Fig. 2). For the sake of clarity, the same points can be also plotted in a 2D space with axes corresponding to the R and B bands: since the information about the real object (satellite) corresponding to each point is conserved, it can be verified that samples of type #1 are spectra from Iapetus and Hyperion, whereas samples of type #2 are spectra from Phoebe (see Fig. 3).

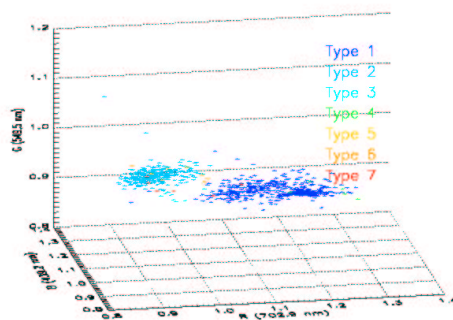


Fig. 2. Normalized reflectances of the samples in the RGB space.

From this classification, which remains essentially unchanged by lowering the confidence level, we can infer that the spectral behaviour of the dark side of Iapetus, in the visible range, is more similar to that of Hyperion rather than to Phoebe. This was expectable, as it is known that the surfaces of Iapetus and Hyperion are both reddish whereas the surface of Phoebe is essentially gray.

6. Results in the Infrared range

In the range measured by VIMS-IR ($0.85 - 5.1 \mu\text{m}$), unlike the visible range case, several absorption features can be identified in the spectra of the three icy satellites. All of the spectra are dominated by the large $3 \mu\text{m}$ absorption band due to the OH fundamental stretch, and the spectral signatures of water ice, trapped CO_2 and other organic compounds can be recognized as well (Clark et al. 2005; Buratti et al. 2005; Cruikshank et al. 2006).

In the past, for classification purposes, we used the spectral range offered by VIMS-IR, both as a whole and truncated at $4.3 \mu\text{m}$ in order to avoid any thermal emission from the three bodies (Tosi et al. 2006). Here we adopt a different approach: instead of normalizing the spectra to one channel and using all of the 256 available spectral channels of VIMS-IR, we measured six band strengths for as many significant absorption bands, and we sampled the continuum level in three different points of the spectrum,

Table 1. Details of the VIMS cubes used in this work. P=Phoebe, I=Iapetus, H=Hyperion

Satellite	Filename	Date	UTC onboard	Spatial dimensions (px)	Spacecraft altitude (km)	Spatial resolution (km/px)	Phase angle (°)
P	V1465674952	11 Jun 2004	19:32	30×18	2100	1.0×0.5	24.6
I	V1483212524	31 Dec 2004	19:03	64×44	123451	61.7×30.8	95.4
H	V1506391910	26 Sep 2005	01:43	24×12	13611	6.9×3.5	49.8

thus considering a total of 9 variables instead of 256. For each absorption feature, the band strength was computed, following the definition by Clark and Roush (1984), as:

$$D = 1 - \frac{R_b}{R_c} \quad (1)$$

where R_b is the reflectance measured at the band center and R_c is the reflectance of the spectral continuum at the band center, reconstructed through a linear fit.

By composing such a dataset and classifying it through the G-mode method with high confidence level (3.0σ), we find again 7 types. By plotting the result in a 3D space with axes corresponding, for example, to the strengths of water ice, trapped CO_2 and $\text{C}\equiv\text{N}$ bands, again two main types can be recognized, made up by 572 and 278 samples, respectively (see Fig. 4). For clarity, the same points can be also plotted in a 2D space with axes corresponding, e.g., to the strengths of water ice and CO_2 . Keeping the information about the real object (satellite) corresponding to each point, we can verify now that samples of type #1 are spectra of Iapetus and Phoebe, whereas samples of type #2 are spectra of Hyperion (see Fig. 5).

The situation in the IR is therefore the opposite with respect to the Vis: on the basis of the band strengths of several absorption features, related to the abundances of the corresponding compounds on the surfaces of the satellites, and of the continuum level sampled in three different points, the degree of similarity is higher between the dark hemisphere of Iapetus and Phoebe. This is understandable since, in the infrared spectra of the three satellites measured by VIMS-IR, some signatures,

which are evident on Iapetus and Phoebe, are absent or very faint on Hyperion.

7. Dust origin

If we accept the result given by the G-mode classification in the IR, i.e., the dark material mantling the leading side of Iapetus is compositionally more similar to Phoebe rather than to Hyperion, then a reasonable dynamical explanation has to be found. To explain the presence on Iapetus of particles from Phoebe, we have to determine:

1. A mechanism for dust generation;
2. A mechanism for the mass transfer;
3. The efficiency of the capture process.

If we follow the scenario originally proposed by Soter (1974), particles from Phoebe spiral towards Saturn due to the Poynting-Robertson effect. Since they are moving inward on retrograde orbits, they collide with the Iapetus' leading side. A natural mechanism for the dust generation is given by impacts: the images of Phoebe acquired by the optical camera onboard the Cassini Orbiter spacecraft evidenced a heavily cratered surface. Moreover, recent results suggest the existence of at least two collisional families among the Saturn's irregular satellites (Turrini et al. 2006). Finally, impacts with micrometeorites make the dust generation a continuous process, even though at a reduced rate.

Dust migration from the region of the irregular satellites to Iapetus is explicable owing to the radiative forces: for dust grains with size $< 1 \mu\text{m}$, the radiation pressure effects rule, whereas for sizes of the order of $1 \mu\text{m}$ the

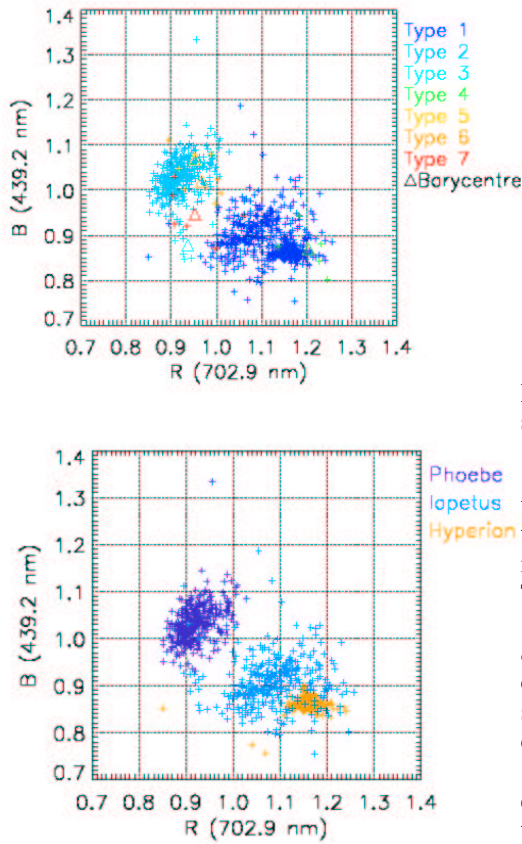


Fig. 3. Normalized reflectances of the samples projected on the RB plane. Above: types isolated by the G-mode. Below: satellites corresponding to the above types.

Poynting-Robertson drag is no longer negligible. By analysing the reflection spectrum of the Saturnian icy satellites acquired by VIMS, it turns out that the typical ice grain sizes on these surfaces range from 1 to 5 μm , comparable to telescopic observations over the last two decades (Hansen et al. 2005). The ranges of variation of both the inclination and eccentricity of dust particles reaching Iapetus have been computed evaluating the structure of the fragment clouds produced by Phoebe for several ejection velocities (30, 50, 100 and 200 m/s). The efficiency of the cap-

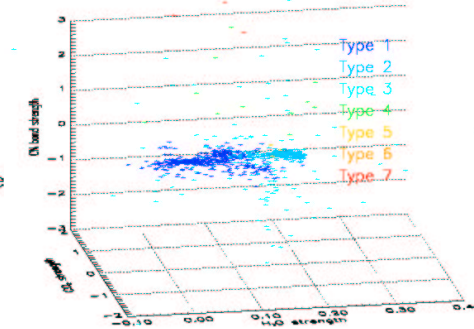


Fig. 4. Classification in the IR. The 3 axes correspond to the strengths of water ice, CO_2 and $\text{C}\equiv\text{N}$.

ture process has been evaluated by computing the collision probability through the Kessler’s method (Kessler 1981).

The capture probability ranges from 10^{-5} to 10^{-6} , with the first value related to orbits with $e \leq 0.1$ and $i \geq 170^\circ$, thus relatively little eccentric and inclined. Assuming perfectly absorbent grains, the decoupling time between dusts’ and Iapetus’ orbits ranges from 10^4 to 10^5 years, with the value increasing with the eccentricity of the dust grains’ orbits. These two effects (capture probability increasing for less eccentric orbits and decoupling time increasing for eccentric orbits) tend to balance each other, producing an almost constant efficiency: for the orbits we considered, the efficiency of the capture process is included between 50% and 80%.

8. Conclusions

The spectral range covered by VIMS allows an analysis of the satellites’ surfaces more complete than in the past. For the three considered satellites, the correlation explored through the G-mode in the visible range is stronger between Iapetus and Hyperion, as expected. However, this result is not conclusive, because similar photometric correlations have been pointed out also with other small dark satellites, moving on both retrograde and prograde orbits. On the other hand, in the infrared range the correlation appears to be stronger be-

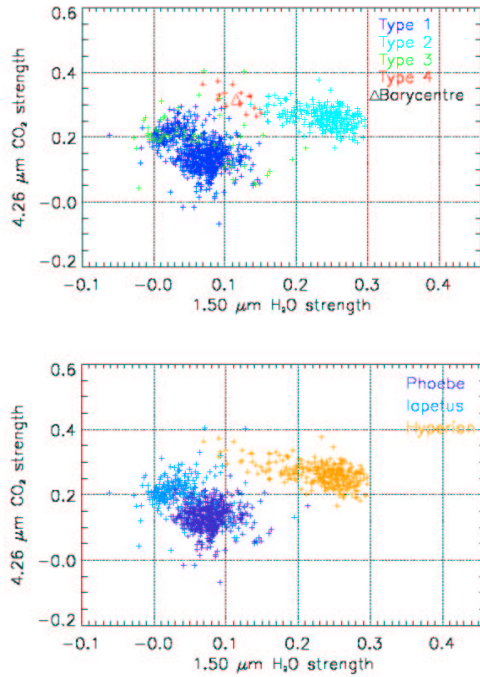


Fig. 5. Classification in the IR. The axes correspond to the strengths of water ice and CO₂. Above: types found by the G-mode. Below: satellites corresponding to the above types.

tween Iapetus and Phoebe, both on the basis of the whole spectrum and of the diagnostic bands' strengths.

The divergent results for the visible and infrared data still has to find a reasonable explanation. In any case, the possibility of dust

on Iapetus coming from Phoebe is explainable in a natural way by combination of the effects of the impacts on Phoebe and the Poynting-Robertson drag. The described process seems to be characterized by a high capture efficiency, making Iapetus an effective shield to the dust penetration in the inner regions of the Saturn system.

References

- Brown, R. H., et al. 2004a, *Space Sci. Rev.* 115, 111-168
- Buratti, B. J., et al. 2002, *Icarus* 155, 375-381
- Buratti, B. J., Hicks, M. D., and Davies, A. 2004, *Icarus* 175, 490-495
- Buratti, B. J., et al. 2005, *ApJ*. Volume 622, L149-L152
- Clark, R. N., et al. 2005, *Nature* 435, 66-69
- Clark, R. N., and Roush, T. L. 1984, *JGR* 89, 6329-6340
- Coradini, A., et al. 1977, *Comput. Geosci.* 3, 85-105
- Cruikshank, D. P., et al. 2006, Submitted to *Icarus*
- Hansen, G. B., et al. 2005, AGU Fall Meeting 2005, abstract #P11B-0124AGU
- Kessler, D. J. 1981, *Icarus* 48, 39-48
- Matthews, R. A. J. 1992, *Quart. J. R. Astron. Soc.* 33, 253-258
- Soter, S. 1974, *IAU Colloq.* 28, Cornell University, August 1974
- Tholen, D. J. and Zellner, B. 1983, *Icarus* 53, 341-347
- Tosi, F., et al. 2006, 37th LPSC, abstract no.1582
- Turrini, D., et al. 2006, *Icarus*, in preparation